International Journal of Fluid Power 3 (2002) No.3 pp. 37-48

DYNAMIC MODELLING AND PARAMETRIC STUDIES OF AN INDEXING VALVE PLATE PUMP

Junhee Cho[1], Xiaoping Zhang[2], Noah D. Manring[3] and Satish S. Nair[3]

[1]Samsung Electronics Co. Ltd., Suwon City, Kyunggi Do, 429-854, Korea
[2]MEMS CAD & Design Engineer, Intpax Co. Ltd., 6 Results Way, Cupertino, CA 95014, USA
[3]Mechanical and Aerospace Engineering Department, University of Missouri - Columbia, Columbia MO 65211, USA
cjunhee@samsung.co.kr, xzhang@intpax.com, ManringN@missouri.edu, NairS@missouri.edu

Abstract

The swash-plate in a variable displacement pump experiences very large forces and moments that try to dislocate its position; therefore, a large device is required for adequate control. In this paper, the dynamics of an alternative pump design using an indexing valve plate to position the swash-plate are reported. The indexing valve plate design is aimed at controlling the pressure transition for a piston, which is moving from a high-pressure port to a low-pressure port. In this paper, the governing equations for the pump are derived and the detailed open-loop and parametric studies, which are necessary for understanding the overall dynamic characteristics of the pump, are reported. Also, full nonlinear and simplified modelling approaches for the system are compared.

Keywords: swash-plate, axial piston pump, indexing valve plate, pressure carry-over

1 Introduction

Since changing the rotational displacement of the swash plate is fundamental for altering the output power of the pump, it is important to understand the moments that are exerted on the swash plate by the reciprocating pistons and any control devices that exist within the pump. The dynamics of these components can often dictate the overall dynamic behavior of the hydraulic system. In the past, various authors have developed mathematical models for such pumps by considering the pressure transients within the piston chambers. Due to the complexity of the pressure transitions between pump ports, some authors have used an approximate pressure-profile schematic to characterize the pressure transitions (Zeiger and Akers, 1985; Schoenau et al, 1990; Yamaguchi and Ishikawa, 1979). Zeiger and Akers developed mathematical models and investigated the effects of different designs, tolerance variations, and varying operating conditions. Manring proposed an approximate pressure distribution and also developed equations for the torque components acting on the swash-plate. He also introduced the pressure carry-over to explain the pressure transition at top and bottom dead centers (Manring, 1998). One simplification for the dynamic model of the axial-piston pump has been introduced by using sensitivity techniques (Kim et al, 1987).

In general, the swash-plate experiences very large forces and moments that try to dislocate its position and therefore a correspondingly large device is required for adequate control. The control device, which biases the pump and is used to stroke and de-stroke the swash-plate, is generally comprised of hydrostatic actuators and springs that overwhelm any other forces acting on the swash-plate. These control mechanisms are generally large, inefficient, and costly to manufacture. In light of these inherent disadvantages of the conventional control mechanism, it is desirable to replace this design altogether with another device that is smaller, less costly, more efficient, and more dynamically responsive.

This paper deals with a mathematical model of the swash-plate using a new control idea, which is called an indexing valve plate. The open-loop system dynamic characteristics of the pump and the indexing valve plate are considered. The indexing valve plate uses the pressurized fluid from the discharge port to rotate the ported geometry of the valve plate about the centerline of the shaft and ports. This alteration in porting locations modifies the pressure characteristics within the pump so as to adjust the swash-plate angle, α, itself. Based upon this concept, the governing equation of motion for the swash-plate is derived with an assumed piston pressure distribution. A simplified model is then

This manuscript was received on 8 July 2002 and was accepted after revision for publication on 9 December 2002

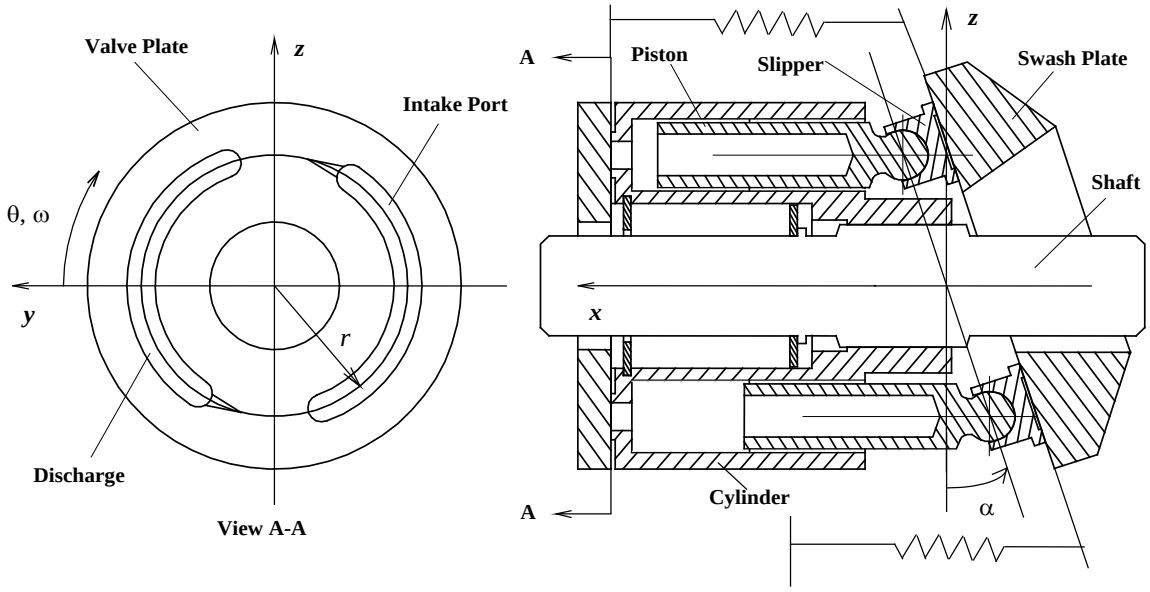

Fig. 1: *General configuration of overall system*

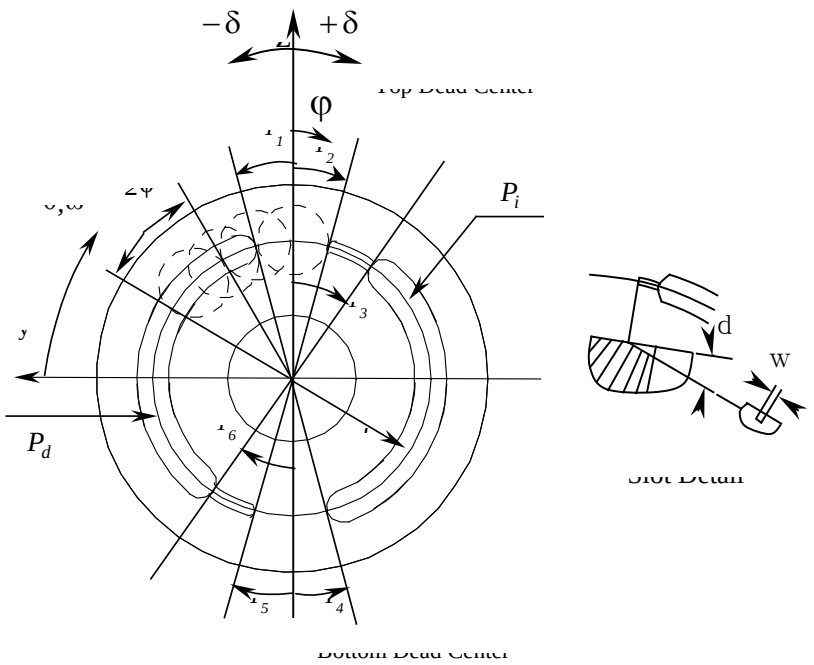

Fig. 2: *Valve plate geometry and slot detail*

developed for the overall dynamics. One relationship between the swash-plate angle and the indexing valve plate angle can be explained by the steady-state analysis. The open-loop studies consist of the investigation of the swash-plate dynamic performance with a given step input and the parametric sensitivity study. The open-loop dynamics of the swash-plate with the system stability is investigated using a linearized version of the reduced order model. The variation effects of both the valve plate and the swash-plate parameters are also investigated using numerical analysis, which is then compared with an analytical result.

2 Governing Equations of Motion

The basic components are shown in Fig. 1. Each pump component is analyzed separately and the major forces are described by the respective free body diagram analysis. The detailed description of this analysis is shown in (Cho et al, 1999). The coordinate systems used depend upon the component considered. Fixed and moving coordinate systems are used whenever necessary and any force analysis is considered only in the *x* and *z*-directions since the pump rotates about the *x*-axis. Since an un-primed coordinate system is attached on the centerline of the pump shaft, a primed

coordinate system describes the centerline of the swash-plate pivot and a double primed coordinate system is fixed at the mass center of the slipper, which translates and rotates together with the slipper.

The moment exerted on the swash-plate about its pivot is given by

$$T_c^{y'} = \Phi_1 \ddot{\alpha} + \Phi_2 \dot{\alpha}^2 + \Phi_3 \dot{\alpha} - \frac{N(M_p + M_s) r^2 \omega^2 \tan(\alpha)}{2\cos^2(\alpha)} + \frac{\sum_{n=1}^{N} A_p P_n (r \sin(\theta_n))}{\cos^2(\alpha)} \quad (1)$$

where

$$\Phi_1 = I'_{yy} + N(I''_{yy} + M_s X_s^2) + (M_p + M_s)\frac{N r^2}{2\cos^4(\alpha)}$$

$$\Phi_2 = N(M_s + M_p)\left(\frac{r^2 \sin(\alpha)}{\cos^5(\alpha)}\right) \text{ and}$$

$$\Phi_3 = \left(\frac{N C_p r^2}{2\cos^4(\alpha)}\right).$$

This model is referred to as the full nonlinear model of the moment exerted on the swash-plate. The pressure summation term in the model can be simplified, and this is discussed in (Zhang et al, 2000).

3 Simplified Model with Indexing Valve Plate

A simplified model for the swash-plate dynamics is developed using the preceding equations and assuming a fixed non-zero valve plate position, i.e., $\delta \neq 0$. The indexing valve plate is aimed at controlling the pressure transition for a piston, which is moving from a high pressure port to a low pressure port. This is based upon the idea that the pressure transition occurs near the top and bottom dead center locations of the piston trajectory, over an average angular distance. By rotating the valve plate relative to its center, this angular distance and location may be modified. Figure 2 also shows the indexing valve plate geometry. In this paper, it is assumed that the diameter of the piston chamber is less than the angular distance between the ports. The valve plate can be indexed in either a positive (in the direction of shaft rotation) or negative direction.

To get an average pressure history, the summation sign in Eq. 1 is replaced by $\frac{N}{2\pi}\int_0^{2\pi}$ and the argument is integrated with respect to θ_n to get the average value of the swash-plate moment with respect to an approximated pressure profile shown in Fig. 3. As shown in Fig. 3, the discharge pressure distributed along the discharge port of the valve plate may be represented as the approximated pressure profile. This approximated distribution of the discharge pressure emphasizes that the piston undergoes a transition in pressure as it passes over the slots on the valve plate, and the transition occurs through some average angular-distance that is referred to as the pressure carry-over angle, γ. By such an analysis (Zhang et al, 2000), the following result is obtained:

$$\frac{\sum_{n=1}^{N} A_p P_n (r \sin(\theta_n))}{\cos^2(\alpha)} = \frac{N A_p^2 r^2 A_{damp}(P_d)}{\pi \cos^4(\alpha)}\dot{\alpha} + \frac{N A_p}{2}\frac{r}{\pi}\sec^2(\alpha)(P_d - P_i)\gamma \quad (2)$$

where γ is the pressure carry-over angle and $A_{damp}(P_d)$ is a damping term due to piston pressure forces:

$$A_{damp}(P_d) = \int_0^{T_3} \overline{\Delta P_n} \cos(\varphi) d\varphi \quad (3)$$

where T_3 is the angular distance from the top dead center to the end of the slot shown in Fig. 2, and $\Delta\overline{P}_n$ is a scaled version of P_n. Using Eq. 2 and 3, one reduced order model of Eq. 1 with an unknown systematic viscous damping coefficient, C_s, may be given by

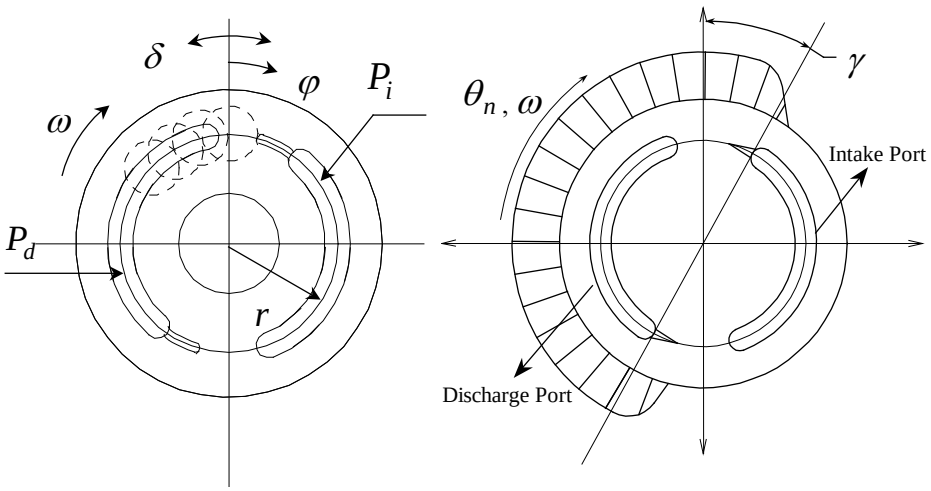

Fig. 3: *Piston pressure characteristics*

$$T_c^{y'} = \Phi_1\ddot{\alpha} + \Phi_2\dot{\alpha}^2 + \Phi_4\dot{\alpha} - \frac{N(M_p + M_s)r^2\omega^2\tan(\alpha)}{2\cos^2(\alpha)} + \frac{N A_p r}{2\pi\cos^2(\alpha)}(P_d - P_i)\gamma \quad (4)$$

where

$$\Phi_4 = \frac{N C_p r^2}{2\cos^4(\alpha)} + \frac{N A_p^2 r^2}{\pi\cos^4(\alpha)} A_{damp}(P_d) + C_s$$

As previously mentioned, the valve plate indexing affects the change of the pressure characteristic at the transient regions, and this pressure change results in the change of the pressure carry-over. This pressure carry-over is obtained from the summation of γ_o (the pressure carry-over angle when the indexing valve plate angle, δ, and the time derivative of the swash-plate angle, $\dot{\alpha}$, are zero at a certain operating pressure condition) and an effective pressure carry-over term due to the valve plate indexing. Based on this idea, it should be considered that a non-zero value of the pressure carry-over angle, γ, produces a moment about the swash-plate pivot axis that is proportional to the working pressure of the pump.

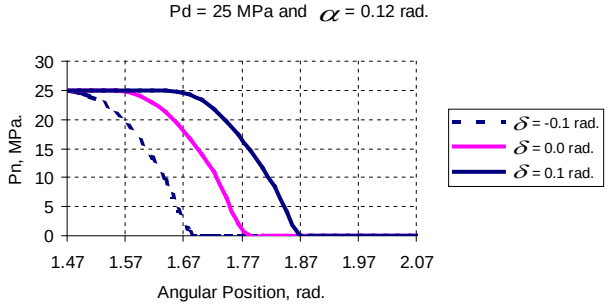

Fig. 4a: *Pressure at top dead center*

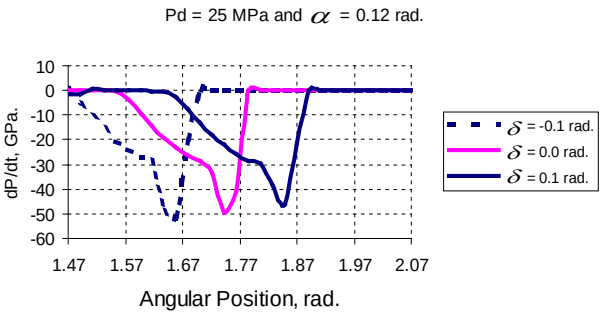

Fig. 4b: *Pressure transition at top dead center*

Since the pressure carry-over angle is a function of the pressure difference at the transient region, Fig. 4 shows the pressure transition at the top dead center with respect to the valve plate indexing. Three different indexing angles are compared when P_d = 25 MPa and the swash-plate angle α = 0.12 radian. The indexing angles are given by δ = -0.1, 0.0, and 0.1 radian. The pressure transition at the bottom dead center with respect to the valve plate indexing has the same characteristics of Fig. 4 in the opposite direction.

To determine the pressure carry-over, γ_o should be calculated first. Since the volumetric changes of the piston chamber are small near the pressure transition region, the time derivative of the piston chamber volume may be ignored. Using Eq. 2 with replacing the summation sign by $\frac{N}{2\pi}\int_0^{2\pi}$, and integrating with respect to θ_n, the pressure carry-over, γ_o, may be calculated as

$$\gamma_o = \frac{1}{(P_d - P_i)}\int_{\frac{\pi}{2}}^{T_3} P_n\cos(\varphi)d\varphi \quad (5)$$

It is assumed that the angular distance between the end point of the discharge port and the beginning point, T_3, of the slot is equal the piston swiped angle, and the pressure transition starts at the top dead center. The integral term shown in Eq. 5 explains one of the swash-plate moment components generated by the piston pressure within Eq. 4, and it can be calculated using numerical methods.

In previous research, the analysis of the pressure carry-over angle did not include the effect of a varying swash-plate angle, α, which can create pressure spikes in the transition region. Furthermore, the numerical comparison for the pressure carry-over shown in Fig. 5 explains that the change of the pressure carry-over is not equal to the change of the indexing angle due to the linearity assumption. Equation 1, 2, and 4 show that the piston pressure effects on the swash-plate moment are proportional to the carry-over, γ. This term must be modelled and controlled correctly in order to achieve adequate control of the pump. Thus, the following simplification may be helpful to understand the relation between the piston pressure and the pressure carry-over and the effect of the pressure carry-over with the indexing valve plate.

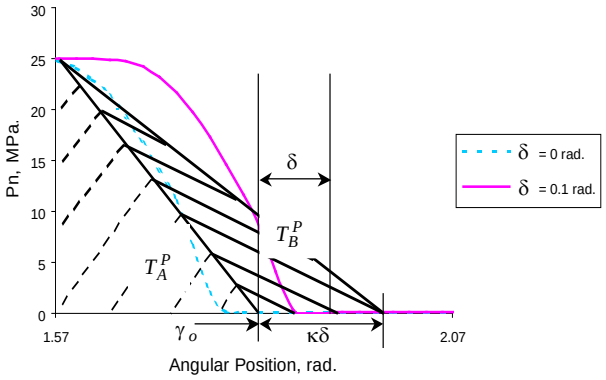

Fig. 5: *Numerical comparison for pressure carry-over*

As shown in Fig. 5, the hatched area with the dashed-line referred to T_A^P shows the moment using the pressure carry-over, γ_o, at δ = 0 and the hatched area with the solid-line referred to T_B^P for the moment using the pressure carry-over, γ, at δ = 0.1 rad. must be added to T_A^P. Based on this investigation, it is noticed that the pressure carry-over angle, γ, for the valve plate indexing may be expressed by the form, $\gamma = \kappa\delta + \gamma_0$, for a more accurate prediction. The coefficient, κ, may be considered as the pressure carry-over efficiency due to

the valve plate indexing, and may be determined by numerical investigations.

When springs are used to bias the pump into stroke (Fig. 1), the spring moment balances the moment in Eq. 4. Therefore, the moment on the swash-plate is equal to the spring moment, i.e.,

$$T_c^{y'} = Pl\,L - k_a L^2 \tan(\alpha) \qquad (6)$$

where the spring pre-load Pl is designed such that $Pl \geq k_a L \tan(\alpha_{max})$. Using Eq. 4 and 6, the swash-plate dynamic equation is given by

$$\ddot{\alpha} = \frac{1}{\Phi_1}\left(Pl\,L - k_a L^2 \tan(\alpha) - \Phi_2\dot{\alpha}^2 - \Phi_4\dot{\alpha} + \Phi_5 - \Phi_6\right) \qquad (7)$$

where $\Phi_5 = \dfrac{N(M_p + M_s)r^2\omega^2 \tan(\alpha)}{2\cos^2(\alpha)}$ and

$$\Phi_6 = \frac{NA_p r(P_d - P_i)}{2\pi\cos^2(\alpha)}\left(\kappa\delta + \gamma_0\right).$$

The reduced order model shown in Eq. 7 will be used for further analysis.

4 Steady-State Analysis

The steady-state refers to any operating condition characterized by a constant rotational speed, ω, of the cylinder-block and a fixed swash-plate angle, α; however, it does not require other aspects of the calculation to remain constant. In particular, the pressure calculations of the piston chambers are continually changing with time. The time derivatives of these quantities, ω and α are therefore set to zero for yielding the steady-state relations. If the time dependencies of α and ω are ignored and the kinematics of the piston-slipper ball-joint (Cho et al, 1999) are considered, the steady-state moments exerted on the swash-plate is given by

$$T_c^{y'} = -\frac{N(M_p + M_s)r^2\omega^2 \tan(\alpha)}{2\cos^2(\alpha)} + \frac{\sum_{n=1}^{N} A_p P_n r \sin(\theta_n)}{\cos^2(\alpha)} \qquad (8)$$

As mentioned previously, the valve plate indexing may generally occur in either positive or negative direction. A positive index is said to occur in the direction of the shaft speed while a negative index is said to occur in the opposite direction of shaft speed. Considering the valve plate indexing, Fig. 6 shows a comparison of the instantaneous moment in Eq. 8 for a single revolution of the cylinder block. From Fig. 6, it is noticed that the instantaneous swash plate moment for a 9 piston pump increases while the valve plate indexing angle increases. Replacing the summation sign shown in Eq. 8 by $\dfrac{N}{2\pi}\int_0^{2\pi}$ and integrating with respect to θ_n, the average torque equation is given by

$$\bar{T}_c^{y'} = -\frac{N(M_p + M_s)r^2\omega^2 \tan(\alpha)}{2\cos^2(\alpha)} + \frac{N A_p r}{2\pi\cos^2(\alpha)}\left(P_d - P_i\right)\gamma \qquad (9)$$

where $\gamma = \kappa\delta + \gamma_0$. Figure 7 shows a comparison of the instantaneous and the average values presented in Eq. 9 for a single revolution of the cylinder block.

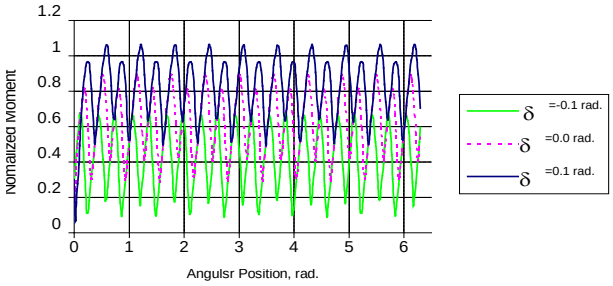

Fig. 6: *Instantaneous moment for a 9 piston with valve plate indexing*

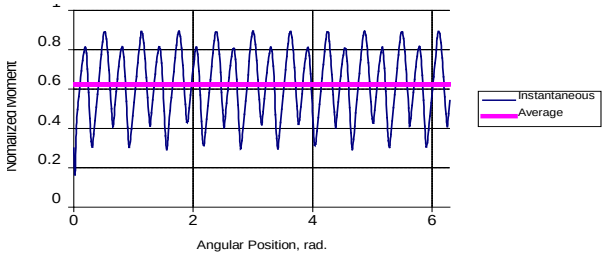

Fig. 7: *Instantaneous and average swash-plate moments for a 9 piston pump*

5 Relationship between γ, δ, and α

The moment acting on the swash-plate is determined by indexing the valve plate, which results in the change of the pressure carry-over angle, γ. This relationship is given by $\gamma = \kappa\delta + \gamma_0$, where κ is the pressure carry-over efficiency due to the indexing valve plate and γ_o is the carry-over angle when $\delta = 0$. To calculate the coefficient, κ, it is necessary to investigate the relationship between the pressure carry-over angle and the swash-plate angle using Eq. 6 and 9. At the steady-state condition for the analytical expression, one relationship between γ and α with the spring moment of the swash-plate may be given by

$$\gamma = \left(\frac{N(M_p + M_s)r^2\omega^2 \tan(\alpha)}{2\cos^2(\alpha)} - Pl\,L + k_a L^2 \tan(\alpha)\right)\frac{2\pi\cos^2(\alpha)}{NA_p r(P_d - P_i)} \qquad (10)$$

Other relationships between the valve plate indexing angle and the swash-plate angle can be obtained using simulation studies. From the full nonlinear model, Eq. 1, the swash-plate angle, α, can be determined by indexing the valve plate using a step input, and this relationship is shown in Fig. 8 at steady-state conditions with various operating points of the discharge pressure.

Using Eq. 10 and the relationship shown in Fig. 8, the pressure carry-over efficiency, κ, can be calculated accordingly, creating no steady-state error between the full nonlinear model and the reduced order model. As shown in Fig. 8, the indexing valve plate can control the swash-plate at any operating condition of the dis-

charge pressure, and it should be noticed that the relationship between α and δ at lower discharge pressure conditions is nonlinear while a relationship between α and δ is nearly linear at high pressures. This means that the selection of κ needs to be careful for lower discharge pressure conditions and κ can be assumed and selected with considering a certain ratio at high discharge pressure conditions.

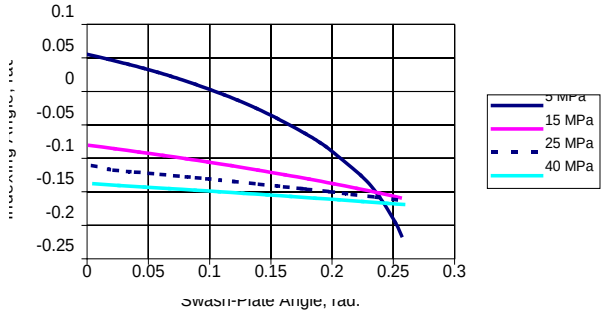

Fig. 8: *Relationship between α and δ*

Since the valve plate is indexed by the control mechanism using a hydraulic actuation system, the indexing angle is limited by the physical pump design, space limitations, the piston reciprocating mechanism, and the pressure characteristics (overshoot, undershoot, etc.). Given these constraints, reasonable valve plate indexing may occur between ± 0.3 rad., and the swash-plate should be controlled within this indexing range for discharge pressures that vary from 5 MPa to 40 MPa. Figure 9 shows the indexing limits at each operating condition of the discharge pressure. The lower line indicates the indexing angle to control the maximum swash-plate angle, 0.253 rad. at the given discharge pressure while the upper line indicates the indexing angle to control the minimum swash-plate angle, 0 rad. at the given discharge pressure.

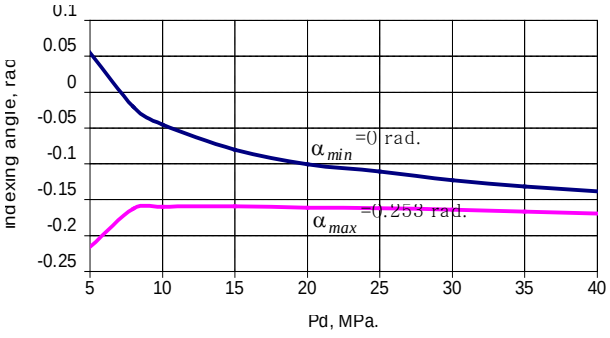

Fig. 9: *Relationship between δ and discharge pressure*

As shown in Fig. 9, the indexing angle varies between -0.22 and 0.05 rad. at 5 MPa and between -0.165 and -0.14 rad. at 40 MPa. Therefore, it can be said that the sensitivity of the valve plate indexing to the swash-plate angle, α, is higher when the operating discharge pressure is increased.

6 Open-Loop Dynamics

The linearized version of the reduced model shown in Eq. 7 about a reference point value (α_o, P_{d_o}, δ_o, and $\dot{\alpha}_0 = 0$) is given by

$$\ddot{\alpha} = \frac{1}{\bar{\Phi}_1}\left(-\bar{\Phi}_4\dot{\alpha} + \frac{(\Phi_7+\Phi_8)}{\bar{\Phi}_1}\alpha - \frac{\bar{\Phi}_6}{(P_{d_o}-P_i)}P_d - \Phi_9\right) \quad (11)$$

where

$$\bar{\Phi}_1 = I_{eff} =$$

$$I'_{yy} + N(I''_{yy} + M_s X_s^2) + N(M_p + M_s)\frac{r^2}{2\cos^4(\alpha_o)}$$

$$\bar{\Phi}_2 = N(M_s + M_p)\frac{r^2\sin(\alpha_o)}{\cos^5(\alpha_o)}$$

$$\bar{\Phi}_4 = C_{eff} = \frac{N C_p r^2}{2\cos^4(\alpha_o)} + \frac{NA_p^2 r^2}{\pi\cos^4(\alpha_o)}A_{damp}(P_d) + C_s,$$

$$\bar{\Phi}_5 = \frac{N(M_p+M_s)r^2\omega^2\tan(\alpha_o)}{2\cos^2(\alpha_o)},$$

$$\bar{\Phi}_6 = \frac{NA_p r(P_{d_o}-P_i)}{2\pi\cos^2(\alpha_o)}(\kappa\delta_o + \gamma_o),$$

$$\Phi_7 = -2\,\bar{\Phi}_2\,(\,P\,l\,L - \,k_a L^2\tan(\alpha_o) - \bar{\Phi}_6 + \bar{\Phi}_5)$$

$$\Phi_8 = \bar{\Phi}_1(-k_a L^2\sec(\alpha_o)^2 + \frac{\bar{\Phi}_5}{\sin(\alpha_o)\cos(\alpha_o)}$$

$$-2\bar{\Phi}_6\tan(\alpha_o) + 2\bar{\Phi}_5\tan(\alpha_o))$$

$$\Phi_9 = \frac{NA_p r(P_{d_o}-P_i)}{2\pi\cos^2(\alpha_o)}\kappa\delta$$

The discharge pressure of the pump is governed by a pressure-rise-rate equation, and this equation is given by

$$\dot{P}_d = \frac{\beta}{V_h}\left(Q_p - Q_{leak} - Q_o\right) \quad (12)$$

where V_h is the volume of the discharge hose, Q_p is the perfect volumetric flow from the pump into the hose, Q_{leak} is the flow from the machine that is lost due to leakage, and Q_o is the volumetric flow demand from the hydraulic circuit. The idealized discharge flow out of the machine is given by

$$Q_p = \frac{N A_p r\alpha\omega}{\pi} = G_p\alpha \quad (13)$$

where G_p is called the pump flow gain. Equation 13 is linearized about $\alpha = 0$ for a convenience even though it is slightly inconstant with Eq. 11.

The leakage flow is a result of low Reynolds number flow conditions and is described by the equation

$$Q_{leak} = K_1 P_d \quad (14)$$

where K_1 is the coefficient of leakage. Using Eq. 13 and 14, the steady-state solution of Eq. 12 yields the following result for the flow demand from the circuit:

$$Q_o = G_p\alpha_o - K_1 P_{d_o} \quad (15)$$

where P_{d_o} and α_o are the desired discharge pressure and the swash-plate angle respectively. Substituting the results of Eq. 13, 14, and 15 into Eq. 12 yields the following pressure-rise-rate of the discharge pressure.

$$\dot{P}_{\mathrm{d}} = \frac{\beta}{V_{\mathrm{h}}} \left(G_{\mathrm{p}}(\alpha - \alpha_{\mathrm{o}}) - K_1(P_{\mathrm{d}} - P_{\mathrm{d_o}}) \right) \qquad (16)$$

By rearranging Eq. 11 and 16 and using reference points of α and P_d, the following state-space form can be developed:

$$\begin{Bmatrix} \ddot{\alpha} \\ \dot{\alpha} \\ \dot{P}_{\mathrm{d}} \end{Bmatrix} = \begin{bmatrix} -\Phi_{10} & \Phi_{11} & -\Phi_{12} \\ 1 & 0 & 0 \\ 0 & \Phi_{13} & -\Phi_{14} \end{bmatrix} \begin{Bmatrix} \dot{\alpha} \\ \alpha \\ P_{\mathrm{d}} \end{Bmatrix} + \begin{bmatrix} \Phi_{15} \\ 0 \\ 0 \end{bmatrix} \delta \qquad (17)$$

where

$$\Phi_{10} = \frac{C_{\mathrm{eff}}}{I_{\mathrm{eff}}} = \frac{\bar{\Phi}_4}{\bar{\Phi}_1}, \quad \Phi_{11} = \frac{K_{\mathrm{eff}}}{I_{\mathrm{eff}}} = -\frac{\Phi_7 + \Phi_8}{\bar{\Phi}_1^2} \quad \text{and}$$

$$K_{\mathrm{eff}} = -\frac{\Phi_7 + \Phi_8}{\bar{\Phi}_1}, \quad \Phi_{12} = \frac{\bar{\Phi}_6}{\bar{\Phi}_1(P_{\mathrm{d_o}} - P_{\mathrm{i}})} \quad \text{and}$$

$$\Phi_{13} = \frac{\beta \ G_{\mathrm{p}}}{V_{\mathrm{h}}}, \quad \Phi_{14} = \frac{\beta \ K_1}{V_{\mathrm{h}}} \quad \text{and}$$

$$\Phi_{15} = \frac{NA_{\mathrm{p}} r(P_{\mathrm{d_o}} - P_{\mathrm{i}})}{2\pi \cos^2(\alpha_{\mathrm{o}})\bar{\Phi}_1} \kappa .$$

The characteristic equation for this system is given by

$$\lambda^3 + (\Phi_{10} + \Phi_{14})\lambda^2 + (\Phi_{10}\Phi_{14} - \Phi_{11})\lambda - \Phi_{11}\Phi_{14} + \Phi_{12}\Phi_{13} = 0 \qquad (18)$$

where the three roots for λ are the system eigenvalues. The eigenvalues may be given by

$$\frac{1}{6}\left(\frac{\Phi_{18} + (2\Phi_{19})^{\frac{2}{3}}}{(\Phi_{19})^{\frac{1}{3}}} \right),$$

$$\left(-48\Phi_{13} \pm \frac{(2^{\frac{4}{3}} + 2^{\frac{4}{3}}3^{\frac{1}{2}}i)(\Phi_{13}^2 + 3\Phi_{14}) + ((-2^{\frac{2}{3}} + 3^{\frac{1}{2}}i)(\Phi_{19}^2))}{12(\Phi_{19})} \right)$$

where $\Phi_{16} = -2\Phi_{13} + (2^{4/3}(\Phi_{13}^2 + 3\Phi_{14}))$,

$\Phi_{17} = (\Phi_{18} + \sqrt{\Phi_{19}})^{1/3}$

$\Phi_{18} = -(2\Phi_{13}^3 + 9\Phi_{13}\Phi_{14} + 27\Phi_{15}\Phi_{16})$ and

$\Phi_{19} = -4(\Phi_{13}^2 + 3\Phi_{14})^3 + \Phi_{18}^2$

The stability criteria of the system may be obtained from Routh's stability criterion. When the discharge pressure is assumed to be a constant value within Eq. 17, two general conditions for the system stability may be obtained as $C_{\mathrm{eff}} > 0$ and $K_{\mathrm{eff}} > 0$. It is noticed that K_{eff} is the function of the spring rate, and a certain limit of the spring rate for the system stability may be calculated from this condition. It yields

$$k_a > \frac{\bar{\Phi}_1\bar{\Phi}_5 \csc(\alpha_{\mathrm{o}})\sec(\alpha_{\mathrm{o}})}{L^2(\bar{\Phi}_1 \sec(\alpha_{\mathrm{o}})^2 - 2\bar{\Phi}_2 \tan(\alpha_{\mathrm{o}}))} - \frac{2(\bar{\Phi}_2(\bar{\Phi}_5 - \bar{\Phi}_6 + Pl\,L) - \bar{\Phi}_1(\bar{\Phi}_6 - \bar{\Phi}_5)\tan(\alpha_{\mathrm{o}}))}{L^2(\bar{\Phi}_1 \sec(\alpha_{\mathrm{o}})^2 - 2\bar{\Phi}_2 \tan(\alpha_{\mathrm{o}}))} \qquad (19)$$

This criterion only explains the minimum of the spring rate for the system stability. The other conditions for the system stability using Routh's criterion can be given by

$$\Phi_{10}^2\Phi_{14} + \Phi_{10}(-\Phi_{11} + \Phi_{14}^2) > \Phi_{12}\Phi_{13} \qquad (20)$$

This expression shows the minimum energy loss from the system since the left side terms within Eq. 20 describes the total energy dissipation of the system. A balance between stability and energy loss must be found and in general this balance results in a damping ratio between the values of 0 and 1. This means that the open-loop system responds in an under damped fashion and will typically exhibit overshoot and oscillation before settling at a steady-state condition. If more energy loss is desired for an improved system response, either increasing the pump leakage or additional damping may be necessary. However, increasing leakage results in decreased pump efficiency. It is therefore less desirable to increase the pump leakage rather than adding damping through another mechanism. The remaining condition for the system stability using Routh's criterion may be written as

$$\Phi_{12}\Phi_{13} > \Phi_{11}\Phi_{14} \qquad (21)$$

Since the term, Φ_{14}, is the function of the leakage coefficient, K_1, the minimum value of the pump leakage coefficient for the system stability can be found from Eq. 21. It should be noticed at this point that the term Φ_{11} is smaller than zero based on the criterion shown in Eq. 19. Therefore, the system stability may not be affected by any values of the pump leakage coefficient. In general, all hydraulic systems have leakage and this helps the system to be more stable. If the pump leakage is considered to satisfy dynamic performance, the pump leakage coefficient is limited by the required pump efficiency. If the pump leakage is ignored, the following condition may be obtained from Eq. 21.

$$\delta > -\frac{\gamma_o}{\kappa} \qquad (22)$$

In practice, the pressure carry-over efficiency, κ, should not exceed the value of 2, therefore, the indexing angle, δ, can only go as half of the pressure carry-over angle, γ_{o}.

For the open-loop dynamic characteristics, consider the pressure rise-rate, Eq. 16. Using Eq. 16 and 17 and Table 1 for the given parameter values, the pole locations are found to be –119.66 and $6.695 \pm 84.13\,i$. The open-loop system is not stable based on the complex conjugate of the eigenvalues. This means that the system fails to satisfy the stability criterion shown in Eq. 20. The damping coefficient, C_{eff}, is given as 11.021 Ns/m at this operating condition.

Table 1: System Parameter Values

Para	Nominal Values	Para	Nominal Values	Para	Nominal Values
I'_{yy}	0.1273 kg m^2	β	1.2x10^3 MPa	k_a	103.4x10^3 N/m
I''_{yy}	1.97x10^{-5} kg m^2	C_d	0.62	A_p	789.2x10^{-6} m^2
M_p	0.3933 kg	C_p	1 N s/m	$A_{s\,max}$	12x10^{-6} m^2
M_s	0.1328 kg	V	65.39x10^{-6} m^3	r	67.31x10^{-3} m
ω	210 rad/s	L	95.25x10^{-3} m	$A_{d\,max}$	386x10^{-6} m^2
Pl	1253 N	N	9		

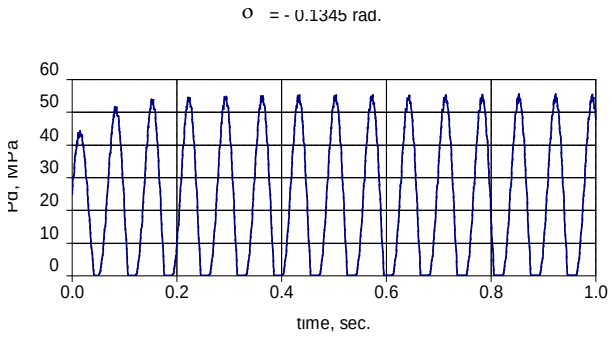

Fig. 10: *Instability response with C_{eff} as 11.021 Ns/m*

Figure 10 shows the response of the unstable system. As shown in Fig. 10, the response is not growing due to the physical saturation limits within the system, and it is found to be about 15 Hz oscillation. From Eq. 20, the minimum value of the damping coefficient, C_{eff}, for the system stability is found to be about 15.121 Ns/m at the given operating condition, and it is little higher than the unstable case, which is 11.021 Ns/m. The corresponding pole locations of that are -135.62 and $-0.108 \pm 79.325\ i$. This means that an additional damping mechanism is required to generate the difference, about 4.1 Ns/m, between the unstable system and the stable system. However, the given operating condition is in the middle range through boundaries, and it may not be sufficient to satisfy the system stability for all possible operating conditions. Two worst cases, almost at the edges within the boundaries, are chosen to find a proper value of the additional damping. During the selection of the additional damping, it should be considered that the system settling time may not exceed more than 1 sec. through the ranges. Based on this, the damping coefficient, C_{eff}, is found to be about 81.021 Ns/m. The corresponding pole locations for the given operating condition are -580.79 and $-15.14 \pm 35.22\ i$. As mentioned previously, the open-loop system responds in an under damped fashion, and Fig. 11 shows a plot of an open–loop response to a given step input at the given operating condition. The saturation limits are not used to modify the response shown in Fig. 11.

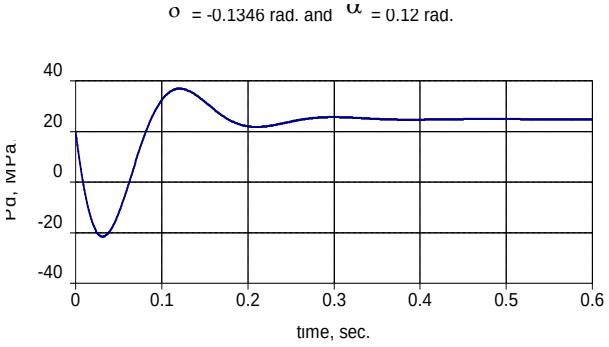

Fig. 11: *Open-loop response*

Based on this analysis, the additional damping coefficient is found to be about 70 Ns/m, and this damping may be obtained by attaching a damping mechanism to the swash-plate spring shown in Fig. 1. In addition, this damping can be replaced by the unknown systematic viscous drag coefficient, C_s. The swash-plate spring equation shown in Eq. 6 may be rearranged as

$$T_c^{y'} = Pl\,L - C_s\dot{\alpha} - k_a L^2 \tan(\alpha) \qquad (23)$$

7 Parametric Studies

The characteristics of the valve plate parameters affecting the pressure transient will be investigated with various slot design criteria and numerical approaches. The variation effect of the swash-plate parameters to both the steady-state results and the dynamic performances will be discussed with the sensitivity analysis.

7.1 Valve Plate Slot Area

Valve plate slot geometry shown in Fig. 2 is a very important design feature of the valve plate since $A_{\text{damp}}(P_d)$ in the reduced order model, Eq. 7, is directly affected by this geometry. The valve plate slots are used to facilitate a smooth pressure transition for each piston chamber as it passes from one port to the next. Without the slots, the pressure rise and drop rates within the piston chambers become unacceptably high. These high-pressure transients produce sudden loading of pump parts and create noisy machines with reduced life characteristics. Several cases of the slot area will be discussed and the characteristics of $A_{\text{damp}}(P_d)$ will be investigated depending upon the slot area change. Since the discharge area, A_o, is the cross-sectional area of the flow passage at the top and bottom dead centers, it varies with the angular dimension, φ. If the time rate-of-change of the fluid volume, V, is ignored near the top and dead centers due to small change in these regions, the pressure rise-rate within the single piston chamber at these regions can be rewritten as

$$\frac{dP}{d\varphi} = \frac{\beta}{V}\,\frac{C_d A(\varphi)}{\omega}\sqrt{\frac{2(P_b - P)}{\rho}} \qquad (24)$$

Equation 24 is a separable differential equation that may be rewritten as

$$\frac{2\beta C_d}{V\omega\sqrt{2\rho}}\int_0^{\varphi} A(\varphi)d\varphi = \int_{P_o}^{P}\frac{1}{\sqrt{(P_b - P)}}dp \qquad (25)$$

where P_o is the pressure in the piston chamber when φ equals zero. The pressure in the piston chamber as it crosses the valve plate slot and its time rate-of-change are given by

$$P = P_b - \left(\sqrt{P_b - P_o} - \frac{\beta C_d}{V\omega\sqrt{2\rho}}\int_0^{\varphi} A(\varphi)d\varphi\right)^2 \qquad (26)$$

$$\frac{dP}{dt} =$$

$$\left(\frac{\beta C_d A(\varphi)}{V}\right)\sqrt{\frac{2(P_b - P_o)}{\rho}} - \left(\frac{\beta C_d}{V}\right)^2\frac{A(\varphi)}{\omega}\int_0^{\varphi} A(\varphi)d\varphi \qquad (27)$$

By taking the first derivative of this with respect to φ, and setting this result to zero, the maximum pressure time rate-of-change for a particular slot can be obtained. Since $A(\varphi)$ depends on the design of the valve plate slot itself, a number of slot area designs using Eq. 26 and 27 can be applied to achieve a certain value of $A_{damp}(P_d)$. In addition, the slot area and the slot geometry directly affect to $A_{damp}(P_d)$ and γ_o. At the pressure transient regions, $A(\varphi)$ can be replaced by A_{smax}, maximum slot area, and φ can be replaced by φ_f, slot length within Eq. 26 and 27. Numerical simulation will be used to investigate the variation effects of the valve plate slot design. For the middle range of the operating condition, P_d = 25 MPa and α = 0.12 radian to investigate the equation of motion of the swash-plate at any slot geometry designs, γ and δ are set to be the same value as 0.033 and -0.1345 radian at any slot designs. Other parameter values are shown in Table 1. A linearly varying slot area is chosen as an initial design, which corresponds to φ_f = 0.1485 rad. and $A_{smax} = 12\cdot10^{-6}$ m^2. From simulations, γ_o can be obtained as 0.262 radian, and Eq. 3 gives $A_{damp}(P_d) = 1.3413\text{x}10^9$ Ns^2/m^5 for this case.

If any other slot designs are considered dependent upon the design priority, either the slot length or the slot area or both, for the same response as the linearly varying slot design, the same operating condition, α = 0.12 rad., δ = 0.1345 rad., and P_d = 25 MPa, should be used for any cases. Table 2 shows a set of comparison with different slot designs, and these results give essentially the same characteristics. The flat bottom and constant width slot design is denoted by Case 1. The linearly varying type, ramped bottom and constant width, is denoted by Case 2. Case 3 indicates ramped bottom and ramped width slot design. The slot geometries used in this analysis are shown in Fig. 12.

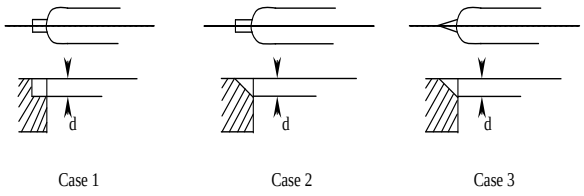

Fig. 12: *A Schematic of common slot geometries*

Table 2: Slot Variation Effects due to Indexing Valve Plate (P_d = 25 MPa and α = 0.12 rad.)

	Case1	**Case2**	**Case3**
A_{smax}	$6.45\cdot10^{-6}$m^2	$12\cdot10^{-6}$m^2	$35.7\cdot10^{-6}$m^2
φ_f	0.173 rad.	0.1485 rad	0.1535 rad.
γ_o	0.287 rad.	0.262 rad	0.275 rad.
κ	1.886	1.7	1.797
$A_{damp}(P_d)$	$1.52\cdot10^9$ Ns^2/m^5	$1.34\cdot10^9$ Ns^2/m^5	$1.1\cdot10^9$ Ns^2/m^5
δ	-0.1345 rad.	-0.1345 rad.	-0.1345 rad.

The result shown in Table 2 is generated from the middle range of the operating point, and Case 2 is set as a reference. Initially, Case 1 and Case 3 have the same slot area and the slot length of Case 2, and the slot area and the slot length may be adjusted to get the same steady state solution of Case 2 at the same operating condition. By comparing the result shown in Table 2, it can be shown that Case 2, a linearly varying slot, can reduce the slot length as compared to the other slots. It can also be shown that Case 3, ramped bottom and ramped width slot design (quadratically increasing slot) requires the largest maximum slot area as compare to the others. In addition, it is noticed that the slot geometry affects γ_o and $A_{damp}(P_d)$ due to the pressure characteristic changes at the transition regions. This means that Case 1 generates the largest $A_{damp}(P_d)$ while Case 3 generates the smallest $A_{damp}(P_d)$. As mentioned previously, the swash-plate damping due to the pressure transition is proportional to $A_{damp}(P_d)$ discussed in the previous sections; therefore, Case 1 provides more damping to the swash-plate than the other slot designs. This behavior is shown in Fig. 13.

Based on this analysis, it can be concluded that the variation of slot geometry affects the dynamic characteristics of the swash-plate at the same steady-state operating condition. Therefore, the slot must be designed by considering the design priority that is most commonly experienced by the pump.

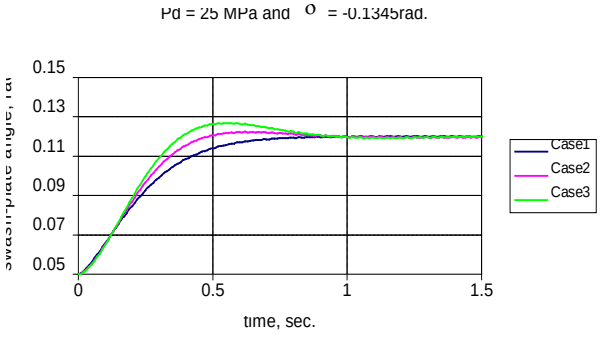

Fig. 13: *Dynamic characteristic changes based on slot geometry*

7.2 Sensitivity Studies

The sensitivity function used in this research is defined as

$$S_{\alpha_j}^{x_i} = \frac{\alpha_j}{x_i} \frac{\partial x_i}{\partial \alpha_j} \tag{28}$$

where $S_{\alpha_j}^{x_i}$ is called as a sensitivity of χ_i with respect to α_j and reflects the influence of the variation of the parameter, α_j, on the state variable, x_i.

The dynamic performance of the system can be investigated using the linearized swash-plate dynamics in Eq. 11 and setting the discharge pressure equal to a constant and the constant term equal to zero, which is given by

$$\ddot{\alpha} + \Phi_{10}\dot{\alpha} - \Phi_{11}\alpha = 0 \tag{29}$$

Therefore, the damping ratio, ζ, for the system is given by

$$\zeta = \frac{\bar{C}_{\text{eff}}}{2\sqrt{\bar{I}_{\text{eff}}\bar{K}_{\text{eff}}}} \tag{30}$$

where $\bar{I}_{\text{eff}} = I'_{yy} + N(I''_{yy} + M_s X_s^2) + N(M_p + M_s)\frac{r^2}{2}$,

$$\bar{C}_{\text{eff}} = \frac{N C_p r^2}{2} + \frac{N A_p^2 r^2}{\pi} A_{\text{damp}}(P_d) + C_s$$

and $\bar{K}_{\text{eff}} = -\frac{N(M_p + M_s)r^2\omega^2}{2} + k_a L^2$.

The sensitivities of the damping ratio for the swash-plate dynamics, with respect to I'_{yy}, $A_{\text{damp}}(P_d)$, and L are given by

$$S_{I'_{yy}}^{\zeta} = -\frac{1}{4}\frac{I'_{yy}}{\zeta}\frac{\bar{C}_{\text{eff}}\bar{K}_{\text{eff}}}{\left(\bar{I}_{\text{eff}}\bar{K}_{\text{eff}}\right)^{3/2}} \tag{31}$$

$$S_{A_{\text{damp}(P_d)}}^{\zeta} = \frac{A_{\text{damp}(P_d)}}{\zeta}\frac{N A_p^2 r^2}{2\pi\sqrt{\bar{I}_{\text{eff}}\bar{K}_{\text{eff}}}} \tag{32}$$

$$S_L^{\zeta} = -\frac{1}{4}\frac{L}{\zeta}\frac{\bar{C}_{\text{eff}}}{\left(\bar{I}_{\text{eff}}\bar{K}_{\text{eff}}\right)^{3/2}\bar{I}_{\text{eff}}k_a L} \tag{33}$$

Similar expressions may be used for the other parameters. The initial damping ratio, ζ, and the natural frequency, ω_n, are found to be 0.68 and 58.3 Hz. The sensitivity of the damping ratio, ζ, to the swash-plate parameters is given in Table 3.

The influence of each parameter on the steady-state value of α_{ss} can be obtained, in a similar manner, using Eq. 11. These are also shown in Table 3. From Table 3, it can be seen that the area of the piston, the piston pitch radius, and the servo arm distance have a significant influence on the swash-plate dynamics, and the pressure carry-over efficiency and that the spring preload affects only the steady-state value of α. In particular, the piston pitch radius, the servo arm distance, and the area of the piston exhibit high sensitivity to the pump dynamics, and so, it should be chosen carefully. In addition, most of the system parameters have a lot of influence on the steady-state solution of the swash-plate, therefore, their tolerances should be kept and managed in reasonable ranges. Even though the pressure carry-over efficiency, κ, is extremely sensitive to the steady-state conditions of the swash-plate, it is related to γ and γ_o, and can be easily adjusted from the steady-state solution of the swash-plate equation. In conclusion, parametric adjustments in this system have the greatest impact on dynamic response as well as steady-state error; therefore, optimizing analysis for these parameters with practical results can be conducted using this technique.

Table 3: Sensitivity of ζ and α_{ss} to Swash-Plate Parameters

Parameters	$S_{\text{Para.}}^{\zeta}$	$S_{\text{Para.}}^{\alpha_{ss}}$
I'_{yy}	-0.454	x
I''_{yy}	-0.0006	x
M_p	0.343	0.755
M_s	0.115	0.255
Pl	x	2.11
$A_{\text{damp}}(P_d)$	0.986	x
r	2.89	0.9
X_s	-0.001	x
ω	1	2.1
k_a	-1	-2.01
A_p	1.97	-1.11
κ	x	7.69
L	-1.098	-1.91

8 Summary and Conclusion

Issues related to dynamical modelling for a valve plate controlled variable displacement pump are reported. The governing equations of motion for the swash-plate have been derived. Since the mathematical model is highly nonlinear and complex, an approximate pressure distribution is used to simplify it. The concept of the pressure carry-over helps to simplify the model, and direct relationship between the valve plate actuation and the pressure carry-over for non-zero δ can be expressed by $\gamma = \kappa\delta + \gamma_o$. A reduced order model is developed and validated. Possible operational envelopes have been discussed for the indexing valve plate pump. Backflow, cavitation, noise, etc. are some critical issues to consider when indexing the valve plate; however, the theoretical simulation studies show that these problems are not so severe due to the small range of the indexing valve plate angle itself. Sensitivity analysis reveals that the variation of porting geometry has a significant impact on the problem. Reduced order modelling results compared very well with a numerical sensitivity analysis using the full nonlinear model.

Nomenclature

A_{damp}	damping area due to piston pressure effects at the pressure transition regions	[Ns^2/m^5]
A_p	effective pressurized area within a single piston	[m^2]
$A_{d\,max}$	maximum discharge area	[m^2]
$A_{s\,max}$	maximum slot area	[m^2]
C_d	orifice discharge coefficient	[-]
C_s	systemic viscous damping coefficient	[Ns/m]
C_p	piston viscous drag coefficient	[Ns/m]
G_p	pump flow gain	[m^3/s]
I'_{yy}	mass moment-of-inertia for the swash-plate	[kg m^2]
I''_{yy}	mass moment-of-inertia for the slipper	[kg m^2]
k_a	spring rate used to bias the pump into stroke	[N/m]
K_1	leakage coefficient	[m^{4}s/kg]
L	spring force moment-arm about the swash-plate pivot	[m]
M_p	single piston mass	[kg]
M_{sw}	the swash-plate mass	[kg]
M_s	the slipper mass	[kg]
N	number of piston	[-]
P_b	boundary pressure outside the control volume of the *n*-th piston bore	[Pa]
P_d	discharge pressure	[Pa]
P_{d_o}	desired discharge pressure	[Pa]
P_i	intake pressure	[Pa]
Pl	spring load when $\alpha = 0$	[N]
P_n	fluid pressure within the *n*th piston chamber	[Pa]
Q_{leak}	leakage flow	[m^3/s]
Q_o	volumetric flow demand from hydraulic circuit	[m^3/s]
Q_p	perfect volumetric flow from pump into hose	[m^3/s]
r	piston pitch radius	[m]
$T_{1\ldots6}$	geometrical dimensions of the valve plate	[rad.]
$T_c^{y'}$	scalar control and containment moment exerted on the swash-plate in the y' direction	[Nm]
V_h	hose volume	[m^3]
X_s	location of the slipper mass center with respect to the center of the piston/slipper ball-joint	[m]
α	swash-plate angle	[rad.]
α_{max}	maximum swash-plate angle	[rad.]
α_{min}	minimum swash-plate angle	[rad.]
α_o	desired swash-plate angle	[rad.]
β	fluid bulk-modulus	[Pa]
δ	indexing valve plate angle	[rad.]
δ_o	desired indexing valve plate angle	[rad.]
γ	pressure carry-over angle	[rad.]
γ_o	pressure carry-over angle when $\dot{\alpha} = 0$	[rad.]
κ	pressure carry-over efficiency due to valve plate indexing	[-]
θ_n, φ	angular coordinate of the *n*th piston	[rad.]
ρ	fluid mass density	[kg/m^3]
ω	rotational speed of the pump shaft and the cylinder block	[rad./s]

References

Zeiger, G., and **Akers, A.** 1985. Torque on the Swashplate of an Axial Piston Pump. *ASME Journal of Dynamic Systems, Measurement, and Control*, Vol. 107, pp. 220-226.

Schoenau, G., Burton, R., and **Kayanagh, G.** 1990. Dynamic Analysis of a Variable Displacement Pump. *ASME Journal of Dynamic Systems, Measurement, and Control*, Vol. 112, pp. 122-132.

Yamaguchi, A., and **Ishikawa, T.** 1979. Characteristics of Displacement Control Mechanisms in Axial Piston Pumps. *Japanese Society of Mechanical Engineers*, Vol. 22, No. 165, pp. 356-361.

Manring, N. 1998. The Torque on the Input Shaft of an Axial-Piston Swash-Plate Type Hydrostatic Pump. *ASME Journal of Dynamic Systems, Measurement, and Control*, Vol. 120, pp. 57-62.

Kim, S., Cho, H., and **Lee, C.** 1987. A Parameter Sensitivity Analysis for the Dynamic Model of a Variable Displacement Axial Piston Pump. *Proceedings of the Institution of Mechanical Engineers*, Vol. 201, No. C4, pp.235-243.

Cho, J., Zhang, X., Nair, S., and **Manring, N.** 1999. Dynamic Modeling of an Indexing Valve Plate Pump. *Proceedings of the International Mechanical Engineering Congress and Exposition*, Nashville, Tennessee.

Zhang, X., Cho, J., Nair, S., and **Manring, N.** 2000. New Swash-Plate Damping Model for Hydraulic Axial-Piston Pump. *ASME Journal of Dynamic Systems, Measurement, and Control*, v123, pp 463-470.

Junhee Cho
Ph. D. Degree of Mechanical Engineering at the University of Missouri – Columbia, USA, 2000. Currently Employee at the Samsung Electronics Co. Ltd., Korea.

Xiaoping Zhang
Ph.D. in Mechanical and Aerospace Engineering in May 2001 from University of Missouri – Columbia, USA. M.S. degree in Automatic Control Engineering in 1994 from Beijing University of Aeronautics and Astronautics at China. Currently working as a MEMS engineer in Intpax Inc. at the Silicon Valley, USA.

Noah D. Manring
Associate Professor of the Department of Mechanical and Aerospace Engineering at the University of Missouri – Columbia, USA.

Satish S. Nair
Professor of the Department of Mechanical and Aerospace Engineering and Associate Dean of Research for the College of Engineering at the University of Missouri – Columbia, USA.